

APPLIED SCIENCES AND ENGINEERING

Fluorescence microscopy visualization of the roughness-induced transition between lubrication regimes

Dina Petrova^{1*}, Bart Weber^{2,3}, Clémence Allain⁴, Pierre Audebert⁴, Cees H. Venner⁵, Albert M. Brouwer¹, Daniel Bonn³

We investigate the transition between different regimes of lubrication and directly observe the thickness of nanometric lubrication films with a sensitivity of a single molecular layer at a multi-asperity interface through fluorescence microscopy. We redefine specific film thickness as the ratio of the lubricant film thickness and the surface roughness measured only at those regions of the interface where the gap is “minimal.” This novel definition of specific film thickness successfully captures the transition from full elastohydrodynamic lubrication to mixed and boundary lubrication. The transition can be triggered by increasing the surface roughness and is accurately predicted by using the new film thickness definition. We find that when the liquid carries part of the load, its apparent viscosity is greatly increased by confinement, and show how the transition between different lubrication regimes is well described by the viscosity increase and subsequent glass transition in the film.

INTRODUCTION

Lubrication has been of interest to society for many centuries; more than 3000 years ago, the ancient Egyptians used lubricants to decrease wear and friction between surfaces. The potential of lubricants for reducing energy consumption is enormous; friction is believed to be responsible for 20% of the world energy consumption (1), and most mechanical systems are lubricated in some way. Lubricated contacts between two rubbing surfaces are usually categorized into three different lubrication regimes. In the elastohydrodynamic lubrication (EHL) regime, the lubricant film is thick enough to completely separate the solid surfaces. In the mixed lubrication (ML) regime, solid-solid contacts penetrate the lubricant film and carry a fraction of the load. In the boundary lubrication (BL) regime, the load is fully supported by solid-on-solid contacts. Friction and wear typically vary by orders of magnitude between the two extremes of the ML regime. Understanding the mechanisms that drive the transition between different lubrication regimes is therefore of paramount importance to control the performance and service life of all components in engineering applications in which a force is transmitted while permitting relative motion. This principle applies both to large-scale applications such as engines, gear boxes (2), or wind turbines (3), and to small scales, in microelectromechanical systems (4) and in biomechanics, for example, in body joints (5).

The implicit dependence of film thickness on the properties of the system comes from hydrodynamics and is only understood for smooth surfaces in the EHL regime (6). In practice, surfaces are not ideally smooth, and lubrication will only be effective if the lubrication film thickness is comparable to or larger than the roughness of the sliding surfaces. The specific film thickness Λ is defined as the

ratio between the average lubrication film thickness h and the root-mean-square roughness of the surfaces S_q : $\Lambda = \frac{h}{S_q}$ (7, 8). The value of Λ then determines the transition between different lubrication regimes, small values corresponding to BL, and large values to EHL (7, 9). However, the transition from EHL to ML is often found to occur at lower values of Λ than anticipated theoretically (10–13). A complicating factor is that surface roughness is measured *ex situ* while the surface may be deformed *in situ* or even exhibit wear. In addition, Λ is defined using the average lubrication film thickness h , while it is predominantly the liquid layer where the surfaces come closest together that is responsible for the lubrication; much of the lubricating liquid remains in the cavities of the surface roughness and does not contribute to the overall effective lubrication. All these factors point to the necessity of performing dynamic and *in situ* measurements of lubricating-film thickness for interfaces that have roughness.

Here, we introduce a fluorescence microscopy method to dynamically image the lubrication layer in three dimensions. We carry out this imaging using a lubricant constituted entirely of fluorescent molecules. Combined with confocal microscopy, we achieve diffraction-limited spatial resolution in the image plane and molecular resolution in the film thickness direction (perpendicular to the surfaces), allowing direct determination of the thickness of the lubricating film in locations where the surfaces are in close proximity to each other. We show that the transition between ML, BL, and EHL is fully controlled by those regions of the multi-asperity contact in which the film thickness is minimal, while the traditional Λ parameter fails to capture the observed transition between lubrication regimes (fig. S7). Our results quantify the crucial role that surface roughness plays in the transition between different lubrication regimes. We show that our findings are material independent and therefore yield new and general insights into lubrication.

On the basis of the new insight into the contact structure provided by our measurements, we also estimate the influence of pressure and viscosity changes on the lubrication in the ML regime. Viscosity increase due to the pressure exerted by the lubricated contacts is

Copyright © 2019
The Authors, some
rights reserved;
exclusive licensee
American Association
for the Advancement
of Science. No claim to
original U.S. Government
Works. Distributed
under a Creative
Commons Attribution
NonCommercial
License 4.0 (CC BY-NC).

¹Van't Hoff Institute for Molecular Sciences, University of Amsterdam, Science Park 904, 1098 XH Amsterdam, Netherlands. ²Advanced Research Center for Nanolithography, Science Park 110, 1090 BA, Amsterdam, Netherlands. ³Van der Waals-Zeeman Institute, IoP, University of Amsterdam, Science Park 904, 1098 XH Amsterdam, Netherlands. ⁴PPSM, ENS Cachan, CNRS, Université Paris-Saclay, 94235 Cachan, France. ⁵Faculty of Engineering Technology, University of Twente, Drienerlolaan 5, 7522 NB Enschede, Netherlands.

*Corresponding author. Email: d.petrova@uva.nl

usually approximated by the pressure-viscosity coefficient in Bair's and Roeland's approximations (12, 14, 15). Under moderate pressures (~0.2 to 0.4 GPa), these approximations predict the viscosity of the liquid to increase by a factor of ~100 during impact and sliding (6, 12, 15). Although it has also been proposed that the liquid might undergo a glass transition during the initial impact (15–17), experimental evidence for this glass transition is very scarce. Our measurements show that the extremely slow squeezing out of the thin lubricant film from the contact under pressure (6) and the transition between different lubrication regimes (12) have the same origin, which is the viscosity increase of the liquid up to the point of the glass transition, with a viscosity increase of many orders of magnitude.

EXPERIMENTS AND RESULTS

We measure the friction coefficient of lubricated contacts as a function of specific film thickness and pressure in the contact region in a sphere-on-plate geometry (Fig. 1A). In the experiment, a droplet of a fluorescent liquid (a liquid made up entirely of fluorescent molecules; Fig. 1B) is placed on top of a flat coverslip that is inserted into the confocal microscopy setup. A sphere, eccentrically attached to a

rheometer plate (Fig. 1A), is lowered into contact with the wetted coverslip until a desired normal force N is reached, which is measured by the rheometer. The contact is then illuminated through the transparent glass substrate by the confocal fluorescence microscope. Because of the low absorption of the fluorescent liquid [1% attenuation of the laser light intensity over a light path of 36 nm as calculated using the Lambert-Beer law ($\lambda_{\text{exc}} = 514$ nm, molar absorption coefficient $\epsilon = 630 \text{ M}^{-1} \text{ cm}^{-1}$ (18))] and the absence of solvent molecules, the fluorescence that is emitted is directly proportional to the number of molecules in the emission volume. If the liquid layer is relatively thin (less than a few hundred nanometers), then the emission volume can be approximated to be a cylinder; in this case, the fluorescence intensity is directly proportional to the local thickness of the liquid layer (19). These measurements then allow the three-dimensional (3D) structure of the lubricating film to be obtained; a single fluorescence image is recorded in 120 ms. The relation between the fluorescence intensity and the gap can be precisely calibrated by comparing the local fluorescence intensities to the locations of the Newton interference rings observed around the contact [see more details in (19)]. This calibration yields an absolute measure of the layer thickness of the lubricating film. A 3D map of the local thickness of the lubricating film can, thus, simply be obtained from the fluorescence intensity

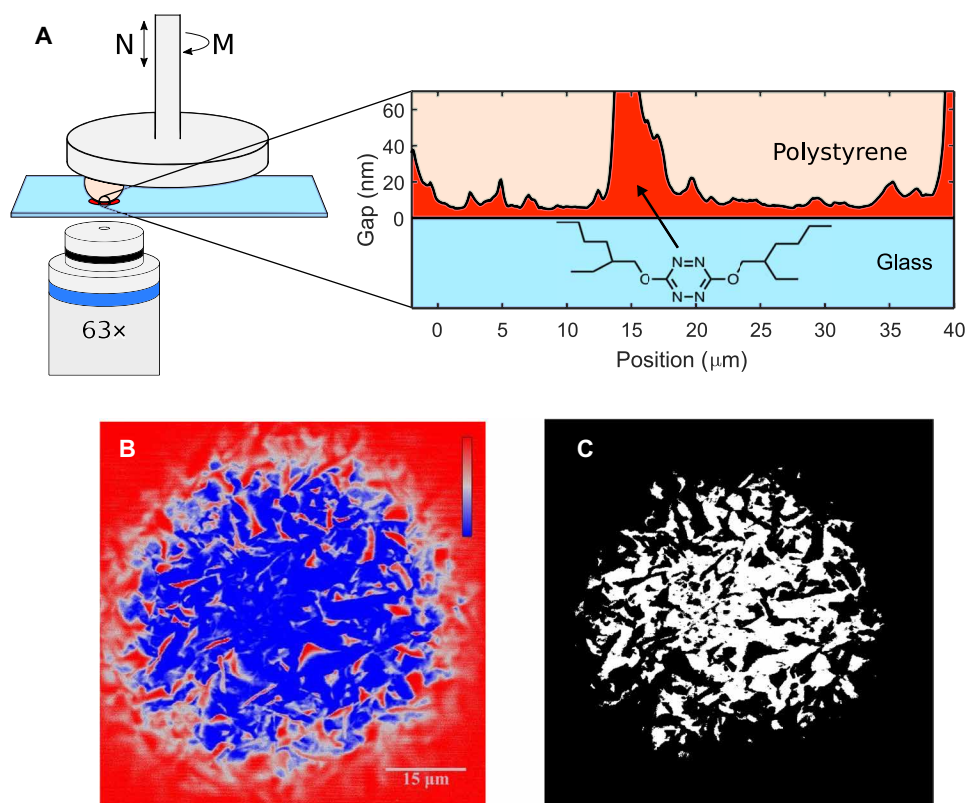


Fig. 1. Fluorescence microscopy imaging of lubricated contacts. Experimental setup (A) and technique (B and C). (A) A rheometer measuring head is mounted on top of an inverted confocal microscope. A float glass coverslip is used as the transparent substrate. A sphere, glued to the rheometer tool, is lowered into contact with the substrate, and the contact is immersed in a fluorescent liquid. By lowering and rotating the rheometer tool, the normal force (F_N) and frictional force can be imposed and measured, respectively. Fluorescence is excited and detected through the transparent substrate using the microscope. In the inset, the molecular structure of the fluorescent liquid 3,6-bis((2-ethylhexyl)oxy)-1,2,4,5-tetrazine is shown (18, 19). Inset: Polystyrene (PS)-on-glass gap profile measured in the EHL regime. (B) Fluorescence intensity image of the contact between a PS sphere and the glass substrate (deconvoluted with the microscope point spread function) pressed with a normal force of 100 mN. The scale bar indicates fluorescence intensity gradient from the lowest (blue) to the highest (red) values. Red regions correspond to gaps filled with fluorescent liquid; blue regions correspond to load-bearing area. (C) Thresholded version of (B); the load-bearing area is shown in white.

image of the contact. The accuracy of measurement of the thickness of the liquid is determined by the shot noise of the detector.

In the BL regime, solid-solid contacts dominate friction. At those locations where the lubricant is completely squeezed out, the fluorescence intensity (and, hence, the film thickness) is zero. Collectively, all areas that do not fluoresce form the area of real (solid-solid) contact that bears the load. The ratio of normal force—imposed by the rheometer—to the area of real contact then gives the average contact pressure in the BL regime, where the lubricant does not bear any of the load. In the ML and EHL regimes, we define the load-bearing area by Otsu thresholding (20) the fluorescence intensities: Only those regions that have intensities (and, thus, gaps) below the threshold are part of the load-bearing area (fig. S9).

To elucidate the interplay between surface roughness, the area of real contact, and various lubrication regimes, we combine in situ fluorescence imaging of the sphere-on-flat interface with sliding experiments using spheres of different roughness. We quantify the roughness of the glass using a confocal scanning profilometer (see Materials and Methods). Compared with spheres, flat glass substrates are very smooth ($S_q \sim 1$ nm). It is well known from contact mechanics that the elastic contact between two rough surfaces is mathematically equivalent to a rough-on-flat interface; in terms of contact mechanics, our rough-on-flat experiment is thus equally meaningful for studying rough-on-rough contacts (21). The glass surfaces do not exhibit any irreversible surface deformations after contact (see fig. S8).

Friction is induced by imposing a constant rotation rate on the rheometer plate that translates into a sliding speed of 10 $\mu\text{m/s}$ for the contact. During sliding, the normal force is kept constant, while the rheometer measures the frictional force. The friction coefficient is then defined as the ratio of the frictional to the normal force, measured for both the dry interface (μ_{dry}) and the liquid-immersed interface (μ) to quantify the lubrication effect of the liquid. We simultaneously measure the load-bearing area and define the average contact pressure as the ratio of the applied normal force and the load-bearing area in all lubrication regimes (Fig. 1 and Materials and Methods).

We quantify the degree of lubrication by comparing the friction coefficients measured for the same spheres either dry (μ_{dry})—without application of the lubricant in ambient conditions—or wetted with the fluorescent liquid (μ). Measuring at constant speed and load, the ratio of the wet and dry friction coefficients μ/μ_{dry} is higher for rough surfaces than for smooth ones (Fig. 2 and fig. S1); in other words, smoother surfaces are more effectively lubricated. High surface roughness corresponds to moderate local contact pressure (Fig. 3). As the sphere surfaces become smoother, the average contact pressure is reduced, and we progressively transit from the high-friction BL regime to the ML and EHL regimes (Fig. 3B).

The average contact pressure at the interface is vital for understanding the observed changes and, hence, also the transitions between different lubrication regimes. Since the load-bearing area is much smaller than the Hertzian contact area of the bulk sphere (20), the pressure in the lubricant film (Fig. 3B) is higher than one would anticipate on the basis of the Hertz contact. That is, in reality, more liquid is squeezed out: The film thickness is smaller than would be anticipated for the Hertz contact, making the transition between EHL and BL occur for smaller loads. This was previously noted by the groups of Mazuyer and Hartl (10, 12). Because we can image both the contact and the thickness of the liquid layer and quantita-

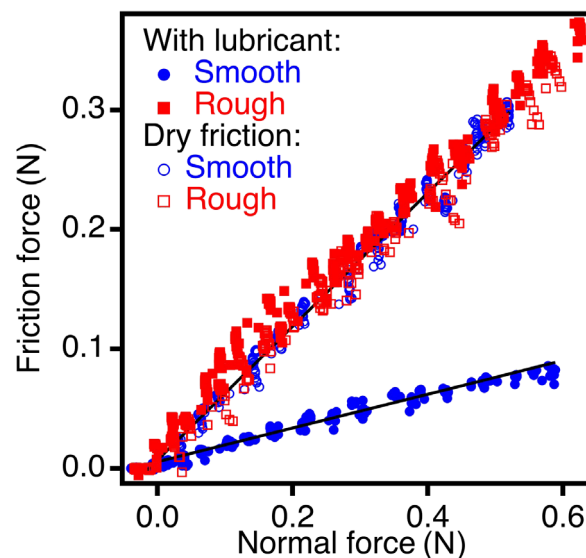


Fig. 2. Friction curves for the roughest and smoothest glass, for dry contacts (open symbols) and lubricated by the fluorescent liquid (filled symbols). Lubrication is observed for the smoothest but not for the roughest glass surface.

tively determine the load-bearing area (Fig. 1C), we can determine and average the specific film thickness over the load-bearing area.

This is defined as “island” specific film thickness $\Lambda_I = \frac{h_I}{S_I}$ where h_I is the average layer thickness within the load-bearing area (in all experiments, the inlet film thickness equals the average film thickness over the load-bearing area; see fig. S9) and S_I is the root-mean-square roughness within the load-bearing area, measured by overlapping the contact and profilometer data (obtained after the friction experiment). This then allows quantifying the film thickness Λ_I only there where it matters. In this manner, we obtain a more general measure that is equally applicable to extremely smooth surfaces (for which the standard definition of Λ suffices) and to very rough surfaces. For the latter, a lot of lubricant is in the valleys of the roughness and does not contribute to the lubrication but is taken into account in the usual definition of Λ . Our main results are shown in Fig. 3B, where we plot the ratio μ/μ_{dry} against the contact pressure and against the island specific film thickness. Different datasets corresponding to different surface roughness all collapse onto a universal S-shaped curve that gives the transition between the different lubrication regimes. The measurements of μ show that a decrease in Λ_I and an increase in the contact pressure lead to an increase in the friction coefficient toward the dry friction coefficient.

To demonstrate how robust this result is for determining the change in lubrication regimes, we test materials other than glass as well. These include polystyrene (PS; which is soft, so it has a small contact pressure) and ruby spheres (which are very hard and therefore exhibit a moderate contact pressure). As shown in Fig. 3B, the results fall on the same curve as the data for glass demonstrating the universal dependence of lubrication on roughness. Thus, we conclude that once the load-bearing area is identified, the results are general in the sense that they do not depend on the material properties. They do not depend on lubricant properties either (see fig. S2), and there is no boundary absorbed lubricant layer present (see Materials and Methods).

To understand these results, we need to find out what determines the film thickness for a given load and sliding speed; if we succeed

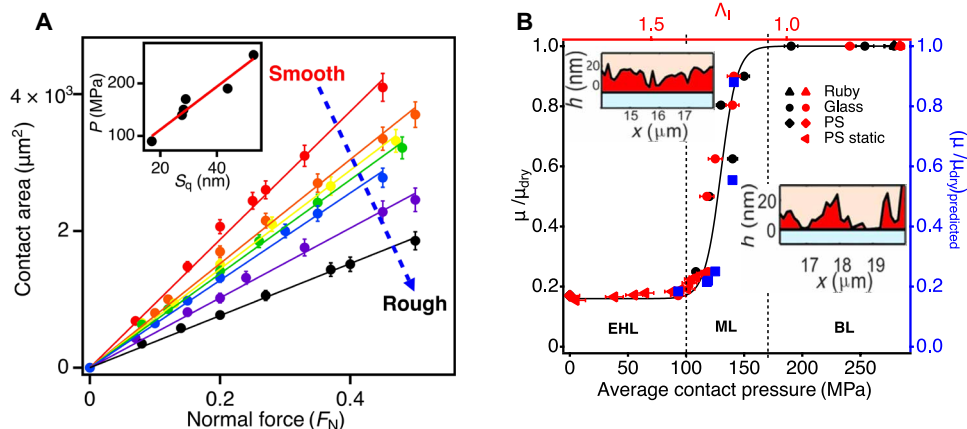


Fig. 3. Transition through lubrication regimes. (A) Contact area as a function of normal force for glass spheres with different roughness. From top to bottom, the roughness increases as indicated by the arrow. In the inset, the average contact pressure is plotted against root-mean-square roughness of the surfaces S_q for a normal force $F_N = 100$ mN. (B) Ratio of lubricated and dry friction coefficients μ/μ_{dry} is plotted against the average contact pressure P_{av} for PS, glass, and ruby (black symbols) spheres measured at $F_N = 100$ mN. The average contact pressure is controlled by surface roughness. The red points for ruby, PS, and glass correspond to μ/μ_{dry} plotted against the island specific film thickness Λ_1 on the top axis. “PS static” points correspond to measurement of μ/μ_{dry} versus Λ_1 with different hold times during which the normal force is fixed but no shear is applied (Λ_1 decreases with time; see below). The black line serves as a guide for the eye. The quantitatively predicted friction coefficient $(\mu/\mu_{\text{dry}})_{\text{predicted}}$ (based on estimation of the viscosity and assumption that there is no significant contribution from dry-on-dry contacts; blue points) is plotted against Λ_1 (top axis). The predicted friction coefficient follows the same trend as the measured data, which implies that the main reason for the transition through the lubrication regimes is the confinement-induced (trapped between two surfaces) change in the viscosity of the lubricant. Insets: Glass-on-glass gap profiles measured in the EHL (left; lubricant film is thick enough to completely separate the surfaces) and BL (right; load is fully supported by solid-on-solid contacts) regimes.

in doing that, then we can predict the friction coefficient when the roughness of the surfaces is known. In particular, the insets in Fig. 4B suggest that for small surface roughness (image on the left, EHL regime), a continuous liquid film separates the sliding surfaces, even though the load-bearing pressures are ~ 50 to 100 MPa. For the largest surface pressure, i.e., the largest surface roughness, some of the asperities penetrate the lubricating film; the observation that the friction coefficient becomes equal to the dry friction case suggests that solid-solid contacts dominate the friction measurement: This is the BL regime. For the intermediate ML regime, the friction coefficient is increasing, but the asperities yet do not penetrate the liquid layer (see Fig. 3B). The question then is by what mechanism the lubricant film resists being squeezed out completely in the ML regime under these moderate pressures.

To investigate whether the lubricant rheology evolves with film thickness, we measure the time evolution of the thickness of an initially thick lubricating layer under an applied load without applying any shear. We, thus, apply a constant normal force $F = 100$ mN and measure the average film thickness within the load-bearing area every few minutes (Fig. 4A). For an incompressible squeezing flow, the thickness of the liquid film can be shown to evolve (22) as

$$h^2(t) = \frac{3\eta D^2 h_0^2}{3\eta D^2 + 16\sigma_0 h_0^2 t} \quad (1)$$

where h is the liquid film thickness; h_0 is its initial value; η is the viscosity of the liquid; D is the diameter of the contact area, derived from the load-bearing area $A: D = \sqrt{4A/\pi}$; t is the time; and $\sigma_0 = 4F/\pi D^2$ is the stress. Unexpectedly, the prediction of Eq. 1 strongly disagrees with the experimental data (Fig. 4A), and we have to conclude that the viscosity evolves during the squeeze out for molecularly thin films at these moderate pressures (22).

The usual assumption is that the effective viscosity of a liquid increases under pressure (17, 22, 23); since Eq. 1 contains no adjustable parameter, we can obtain the instantaneous viscosity from the instantaneous thinning rate and determine how the viscosity changes with film thickness. If we assume the viscosity in Eq. 1 to be variable, we obtain the variation shown with the red symbols in Fig. 4A, with a viscosity that increases significantly and continuously in time while the layer becomes thinner and thinner. Thus, the viscosity increase is not purely a pressure effect; as the gap decreases while the pressure remains the same, we still observe a viscosity increase. We conclude that by confining the lubricant, we induce a continuous increase in its viscosity with increasing confinement. To understand how this viscosity increase affects the friction, we impose frictional slip on the contact after varying waiting times. We find that by imposing slip, the film thickness is not affected at the experimental velocities. Furthermore, the measured friction coefficient increases as the film thickness decreases (Fig. 3B for PS static and Fig. 5A); both viscosity and friction go up as the film thickness decreases.

The friction measurements essentially form an independent measure of the effective viscosity of the lubricant in an independent sliding experiment. Plotting the shear stress (calculated from the friction force and contact area size) as a function of the shear rate (calculated through the speed of sliding and the average thickness of the film) (Fig. 5B), we obtain a straight line that, to a reasonable approximation, goes through the origin. This shows that the behavior of the lubricant is Newtonian; the slope of the stress versus shear rate plot is, then, the viscosity (see Fig. 5B). We find it to be in agreement with the squeezing experiments: From the slope (Fig. 5B), we find $\eta \sim 3.5 \times 10^4$ Pa s when the onset of sliding is after 20 min; in the squeezing experiment (Fig. 3B), we find a similar value for the same waiting time (20 min): $\eta \sim 1 \times 10^4$ Pa s.

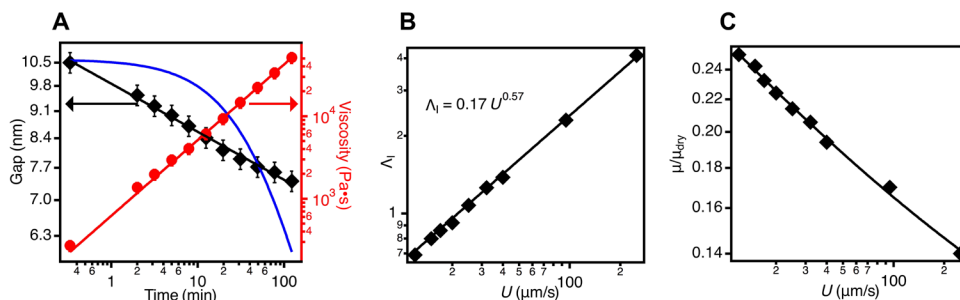


Fig. 4. Evolution in time of the thickness of the fluorescent liquid layer squeezed between the rough PS bead and glass coverslip with a normal force of 100 mN. (A) Average gap between the surfaces versus time (black points). Fit (blue line) according to Eq. 1 with viscosity as the only free parameter; the value found $\eta = 2000$ Pa·s is much higher than that measured using a rheometer: $\eta = 58$ mPa·s (18). Calculated viscosities (red points) derived from the thinning rate according to Eq. 1 as a function of time. (B) Island specific film thickness (Λ_1) as a function of the sliding speed U for rough PS beads on glass. Λ_1 scales with speed according to a power law with exponent 0.57 ± 0.01 . (C) Ratio of wet and dry friction coefficients μ/μ_{dry} as a function of the sliding speed U for rough PS beads. The solid line serves as a guide for the eye.

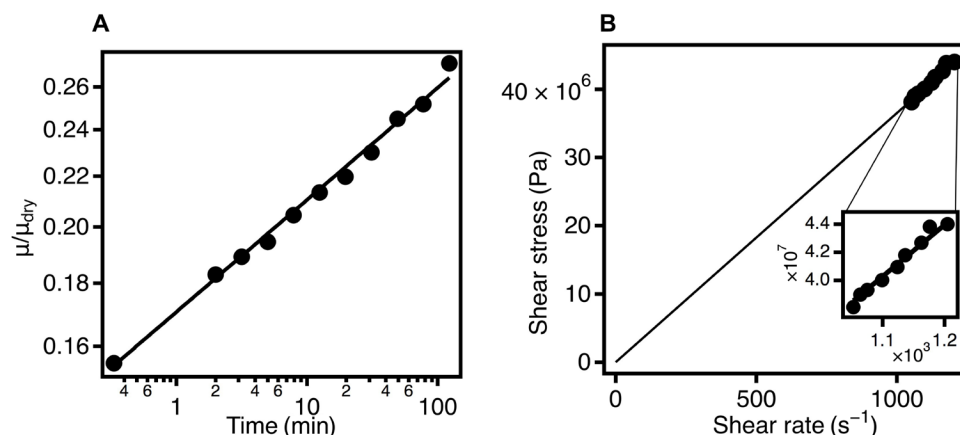


Fig. 5. Static and dynamic properties of the liquid squeezed between PS sphere and a glass coverslip. (A) Friction coefficient (sliding with $10 \mu\text{m/s}$) as a function of waiting time at $F_N = 100$ mN. Although the dry friction coefficient is also time dependent (32), the variation in friction with time for the lubricated experiment is much stronger. (B) Shear stress as a function of the shear rate as obtained by increasing the speed of sliding (after a waiting time of 20 min). The slope of the solid line is the viscosity of the liquid $\eta = 3.5 \times 10^4$ Pa s, which agrees fairly well with the value found in Fig. 3A ($\eta = 1 \times 10^4$ Pa s), for a speed of $10 \mu\text{m/s}$ and a waiting time of 20 min, confirming the validity of our model.

Since our lubricant remains Newtonian, we can now estimate the influence of the sliding parameters on the lubricant, allowing to see how the different lubrication regimes emerge. In the thin lubrication layer, there is a competition between the viscous stress that keeps the film in place and the normal force that squeezes it out. The sliding itself increases the viscous force separating the two surfaces and, hence, leads to thicker films. We quantify this effect in Fig. 4 (B and C) for experimental parameters that we identified as being in the EHL regime: In Fig. 4 (B and C), we show the measured specific film thickness Λ_1 and friction coefficient against sliding speed. Λ_1 indeed increases with increasing speed, causing the friction coefficient to decrease. The power law increase in the film thickness with sliding speed is exactly what is predicted in the absence of surface roughness (13) for the EHL regime, with a power ~ 0.6 ; we find that within the experimental accuracy, our results cannot be distinguished from this prediction (Fig. 4B). The agreement between the Hertzian prediction and our multi-asperity experiment, thus, suggests that each of the islands is in a micro-EHL environment (13), and the regime of lubrication for the whole contact simply scales as that of individual islands. The implication is that the lubrication behavior of a fairly

complicated rough contact can be predicted on the basis of the lubrication theory in (12) for smooth surfaces, using the island specific film thickness. This also holds for other materials with different roughness; for lubricated smooth PS beads, see Fig. S4.

So far, we understand the nature of the EHL regime; the remaining question is how the transition between EHL and BL takes place. From the correlation between friction and viscosity observed in Fig. 5, it may be that for very thin films, the lubricant becomes (almost) solid because it approaches its glass transition. To see whether solidification of the film can explain the increasing friction in the ML regime, we extrapolate the relation between the viscosity and island specific film thickness (fig. S5), and we find that for $\Lambda_1 \sim 0.7$ the viscosity reaches 10^{13} Pa s, which is the IUPAC (International Union of Pure and Applied Chemistry) definition of a glass (24). We find that the ML regime where the friction increases with decreasing specific film thickness can be quantitatively explained by the viscosity increase in the lubricant film (blue symbols in Fig. 3B), down to film thicknesses of $\Lambda_1 \sim 1.2$. For even smaller film thicknesses, the viscosity increases so much that the predicted μ becomes higher than the dry solid-on-solid friction, which is physically unrealistic. Therefore, we conclude that almost

down to $\Lambda_1 \sim 1$, an increase in the confinement-induced viscosity describes the data well; for even thinner films, solid-on-solid friction takes over. In this case, the gap size becomes in the order of 1 to 3 nm, corresponding to only a few molecules (between two and five) in the gap.

The effect of the surface roughness can then also be understood: The higher the roughness, the higher the pressure for a given load and, hence, the higher the viscosity in the lubricating layer. Thus, the local pressure is a crucial factor to be taken into account in lubrication studies of real rough surfaces. Our contact pressures here are calculated on the asperity level using the measured real contact area. Similar observations have been made on atomically smooth mica surfaces, where it is almost impossible to squeeze out the last layers of the liquid (16). We find that under pressure, the viscosity of the liquid increases and that this is the main cause of the increase in the friction coefficient. Under moderate pressures, the liquid approaches its glass transition. This does not exclude the possibility of a complete squeezing out of liquid in the BL regime; it just makes it difficult.

The new method that we introduced for imaging thin films is compatible with most materials, except for those with extreme fluorescence quenching abilities (in particular metals, unless covered by sufficiently thick oxide layers) and polymers with insufficient cross-linking, as the fluorescent liquid can potentially dissolve them. These results contribute to a better understanding of many thin film-related problems, such as antiwear coatings and additives in friction (9, 25), rupture propagation in earthquakes (26), lubrication of prosthetic and cartilage implants in biology (5, 27, 28), and many other problems in lubrication and material science (2, 29).

MATERIALS AND METHODS

Microscopy

To derive the gap between the surfaces through the intensity, the confocal microscope was turned into reflection mode. Reflection of the laser from the bead surface forms an interference pattern known as Newton rings. The maximal intensity of the reflection will occur when the distance between the surfaces is

$$d = \left(m + \frac{1}{2}\right) \frac{\lambda}{2n} \quad (2)$$

where $m = 0, 1, 2, 3, \dots$ is the ring number, $\lambda = 514$ nm is the excitation wavelength, and $n = 1.484$ is the refractive index of the fluorescent liquid. Thus, correlation between intensity and thickness is obtained by taking and comparing a cross section of the fluorescence intensity image and that of the laser reflection image. For details, see (19).

Confinement-induced refractive index change

The refractive index of the fluorescent liquid can potentially change when the liquid is confined. According to the model in (30), the expected change in refractive index with confinement is minimal (<1%) for film thicknesses larger than 10 nm. The potential change in refractive index increases to 10% for thinner films. This change can then result in an uncertainty in the gap measurements of up to 10%. Our conclusions are not affected by this uncertainty.

Equipment

A rheometer (Anton Paar DSR 301) was mounted on top of an inverted confocal microscope (Zeiss Axiovert 200M). We glued a

sphere to the rheometer plate and made contact with the fluorescent liquid. The rheometer measures the normal force on the contact. The fluorescent liquid was excited by an argon ion continuous wave laser at 514 nm. The objective lens is a 63×1.3 numerical aperture LD A-Plan (Zeiss). The filter sets used for filtering of excitation and emission light are dichroic mirror HFT 405/514 and emission filter BP 560|615. Imaging was performed using the Zeiss LSM 5 LIVE microscope control system.

Materials

Smooth glass beads were purchased from Sigmund Linder (type P; borosilicate; radius, 3.175 mm). Smooth PS spheres were purchased from Cospheric (radius, 600 μm). Glass coverslips were purchased from Thermo Fisher Scientific thickness 1.4H. Spheres were inserted in a container with 240-grit sandpaper walls and then shaken for variable number of hours to obtain surfaces with different roughness. The fluorescent liquid was prepared as described in (18). It was purified with a Serlabo prestacked 220-g silica column and a LPLC (low-pressure liquid chromatography) device (Serlabo) using pressures up to 100 psi, which allows the efficient purification of 5 to 10 g of tetrazines.

Plain strain moduli for the experimental interfaces

We previously measured (31) the plain strain moduli for the interfaces that were studied here: glass-on-glass, $E^* = 25$ GPa; PS-on-glass, $E^* = 3.7$ GPa; and ruby-on-glass, $E^* = 54$ GPa.

Surface cleaning

Glass surfaces were rinsed with Hellmanex solution, Milli-Q water, and ethanol (EtOH) three times. After that, they were blow dried under a nitrogen flow. PS and ruby spheres were rinsed using Milli-Q water and EtOH three times, followed by nitrogen flow drying.

Roughness measurement

Roughness measurements were done using a 3D laser scanning microscope (KEYENCE VK-X-1000). Surface roughness S_q was measured after the sliding experiments and calculated as the root-mean-square height variation over an area of 150 μm by 100 μm measured at a resolution of 108 nm per pixel. Because S_q can depend sensitively on the cutoff length and sampling rate, we vary the resolution and size of the measurement area (fig. S10).

Friction

The rheometer measures the torque on the plate to which the sphere is glued. By measuring the radius of the rotation of the sphere with 1% accuracy, we calculate the friction force. Friction tests were performed on PS and the same glass cover slides as in the case of imaging.

Contact area and load-bearing area size and average thickness of liquid layer calculation

To estimate the contact area using the fluorescent liquid, the original image of contact area was deconvoluted with the point spread function by using the ImageJ Iterative Deconvolution software. To calculate the average thickness of the liquid layer between the sphere and the coverslip, intensities were converted into gaps by comparing a fluorescence intensity image with the reflection of the laser light from the bead (Newton rings; see Materials and Methods). Last, values of the height of the pixels corresponding to the contact area were averaged (derived from the thresholded image).

Slope, root-mean-square roughness of the surfaces, and pressure

We found that the average slope of the surface measured using the KEYENCE profilometer is proportional to the roughness for different materials (see fig. S3). As contact pressure is proportional to the roughness (inset Fig. 3A), either of the following parameters can be used for characterization of the transition through lubrication regimes: surface slope, S_q , or contact pressure. Note that the average surface slope depends on the measurement resolution and that S_q depends on the overall scan area size.

The average slopes of the surfaces were calculated using the central difference gradient method programmed in MATLAB. The root-mean-square roughness was also calculated using MATLAB. In fig. S3, average slopes of the surfaces for different materials are plotted against the root-mean-square roughness.

Average thickness measurement during sliding

As the image acquisition time is 100 ms and the sliding speeds range from 1 to 200 $\mu\text{m/s}$, the images of the bead during sliding can be slightly distorted. Distortion happened because the confocal microscopy setup scanned the image line by line and there was a certain delay time between each of the lines. Thus, the load-bearing area appears elongated along the sliding axis. As averaging of the thickness of the liquid happens within the load-bearing area, the average thickness measured during sliding was averaged over 100 ms (the image acquisition time).

Connection between theory and experiment

In fig. S4, we presented the island specific film thickness as a function of speed for smooth PS beads. Thus, we have a connection between theory for smooth surfaces [Snoeijer-Eggers-Venner theory (32), fig. S4 experimental] and theory for rough surfaces (Fig. 4B).

Viscosity as a function of specific film thickness

We plot the viscosity derived from the time-resolved film thickness measurement as a function of the island specific film thickness measured during time-resolved measurements of the friction coefficient (fig. S5A). To estimate whether the viscosity increase is the main reason for the change in friction coefficient, we extrapolated our results for our whole experimental range of Λ_I (see fig. S5B).

Predicted friction coefficient

The ratio between wet and dry friction coefficients was calculated on the basis of the assumption that the contribution of dry-on-dry contacts to the wet friction coefficient was negligible. Shear stress in the liquid is equal to shear stress in the material. Thus, $\tau = \frac{F}{A} = \frac{\mu F_N}{A} = \eta \frac{U}{h}$. This way, we found a relation for the friction coefficient

$$\mu = \eta \frac{UA}{hF_N} \quad (3)$$

where η is the estimated viscosity, U is the sliding speed, A is the load-bearing area, h is the average thickness of the liquid, and F_N is the normal force.

As the viscosity was estimated on the basis of Λ_I and to compare data with the measurements in Fig. 3B, we plot the predicted ratio of dry and wet friction coefficients as a function of Λ_I (see fig. S6).

Plasticity in glass-on-glass contacts

A rough-on-smooth interface at which the surface roughness is deformed purely elastically can, in principle, contain contact area structure down to the molecular scale (33). We analyzed the PS-on-glass contact mechanics in detail and show in (20), (31), and (32) that for this particular system, all contact area structure can be resolved by microscopy because of the large plastic deformation that occurs in this system.

To investigate the presence of this plasticity in our glass-on-glass contacts, we performed experiments (fig. S8) in which we imaged the surface roughness on the glass sphere before and after it was pressed onto the glass substrate. These experiments do not reveal plastic deformation. We think that this result is consistent with the fact that by tailoring the roughness of the glass spheres, we can manipulate the lubrication behavior: If plasticity were to flatten this roughness such that the contact pressure was equal for all glass spheres, then we would not expect to measure a difference in the lubrication properties.

In the lubrication experiments, we observed that by plotting the ratio of wet/dry friction versus the ratio of film thickness/roughness, all data collapsed onto a master curve. This result strongly suggests that the microscopy observations are sufficiently detailed to capture the roughness-induced transition between the various lubrication regimes. We suspected that the lubricating film itself made the experiments less sensitive to the tiniest roughness variations that can, in principle, dominate the dry, elastic contacts. We observed lubricant films of the order 10 nm and surface slopes of the order 0.2. Dividing this film thickness by the slope, we obtained a lateral scale of 50 nm, not that far from the lateral scales that were resolved in the visualization experiments. Furthermore, the method by which we roughened the glass spheres was essentially abrasive wear as a consequence of high-speed impact on sand paper grains (31). The roughness variations between different spheres, created by using different times of roughening with sand paper, likely manifest themselves at those scales that are resolved in the microscopy experiments.

Calculation of the average contact pressure

The average contact pressure was calculated from the applied normal force and size of the load-bearing (or contact) area, derived from the imaging experiments. To derive the load-bearing area size, we thresholded the histogram of the deconvolved images (see example of the deconvolved image and intensity histogram in fig. S9, A and B) using an Otsu threshold (34).

Fluorescent liquid adsorption

To test whether the fluorescent liquid adsorbs onto the experimental surfaces, we first performed a “dry” and a lubricated friction experiment with one particular glass sphere. We then gently cleaned the used glass sphere, which was covered in fluorescent liquid, with EtOH and acetone. Subsequently, we again measured the dry friction between this sphere and a clean and dry glass substrate. The friction coefficient that we found was equal to that measured initially, confirming that there was no adsorbed layer of fluorescent liquid left that influenced the sliding. The same experiment for PS-on-glass contacts gave the same result.

Change of dry friction coefficient with roughness and waiting time

The dry friction coefficient increased with waiting time, as mentioned in (35). The change in the dry friction coefficient within the time

window of measurement was only a few percent (1.05×), while the change in the lubricated friction coefficient was almost two times compared with the initial value. Thus, we neglected the change of the dry friction coefficient with time in our measurements.

The dry friction coefficient increased by only a few percent with increase in roughness. Meanwhile, the change in lubricated friction coefficient (Fig. 3B) was almost fivefold. Thus, the change of the friction coefficient with roughness can be neglected. Currently, we are studying these phenomena in more detail.

SUPPLEMENTARY MATERIALS

Supplementary material for this article is available at <http://advances.sciencemag.org/cgi/content/full/5/12/eaaw4761/DC1>

Fig. S1. Friction curves for different materials, for dry contacts (open symbols) and lubricated by a fluorescent liquid (filled ones).

Fig. S2. Friction curves for glass with variable roughness S_q lubricated by different liquids.

Fig. S3. Average surface slope versus roughness for different materials.

Fig. S4. Evolution with speeds of the thickness of the fluorescent liquid layer squeezed between the smooth PS bead and glass coverslip with a normal force of 100 mN.

Fig. S5. Viscosity as a function of island-specific film thickness Λ_i .

Fig. S6. Predicted friction coefficient (μ/μ_{dry})_{predicted} as a function of island specific film thickness Λ_i .

Fig. S7. Ratio of lubricated and dry friction coefficients μ/μ_{dry} is plotted against the Hertzian contact pressure P_{Hertz} (bottom axis, black points) and standard Λ (top axis, red points) for the same data as in Fig. 3B.

Fig. S8. Glass sphere surface (measured using a profilometer) before contact and after contact.

Fig. S9. Load-bearing area of the lubricated contact between a glass sphere and a glass coverslip.

Fig. S10. Quantification of surface roughness.

Fig. S11. Fluorescence intensity image of a sphere on a glass substrate lubricated by a fluorescent liquid.

Fig. S12. The roughness-induced transition between lubrication regimes.

Fig. S13. Correlation between average contact pressure and island specific film thickness.

REFERENCES AND NOTES

- K. Holmberg, A. Erdemir, Influence of tribology on global energy consumption, costs and emissions. *Friction* **5**, 263–284 (2017).
- L. Dobrenizki, S. Tremmel, S. Wartzack, D. C. Hoffmann, T. Brögelmann, K. Bobzin, N. Bagcivan, Y. Musayev, T. Hosenfeldt, Efficiency improvement in automobile bucket tappet/camshaft contacts by DLC coatings—Influence of engine oil, temperature and camshaft speed. *Surf. Coatings Technol.* **308**, 360–373 (2016).
- C. M. C. G. Fernandes, P. M. T. Marques, R. C. Martins, J. H. O. Seabra, Film thickness and traction curves of wind turbine gear oils. *Tribol. Int.* **86**, 1–9 (2015).
- X. Fan, L. Wang, Graphene with outstanding anti-irradiation capacity as multialkylated cyclopentanes additive toward space application. *Sci. Rep.* **5**, 12734 (2015).
- S. A. H. de Vries, M. van Doeselaar, H. J. Kaper, P. K. Sharma, K. Ito, Notochordal cell matrix as a bioactive lubricant for the osteoarthritic joint. *Sci. Rep.* **8**, 8875 (2018).
- J. Fryza, P. Sperka, M. Kaneta, I. Krupka, M. Hartl, Effects of lubricant rheology and impact speed on EHL film thickness at pure squeeze action. *Tribol. Int.* **106**, 1–9 (2017).
- L. Ma, J. Luo, Thin film lubrication in the past 20 years. *Friction* **4**, 280–302 (2016).
- B. J. Hamrock, S. R. Schmid, *Fundamentals of Fluid Film Lubrication* (Marcel Dekker, ed. 2, 2004).
- D. Gonçalves, A. Vieira, A. Carneiro, A. Campos, J. Seabra, Film thickness and friction relationship in grease lubricated rough contacts. *Lubricants* **5**, 34 (2017).
- T. Zapletal, P. Sperka, I. Krupka, M. Hartl, The effect of surface roughness on friction and film thickness in transition from EHL to mixed lubrication. *Tribol. Int.* **128**, 356–364 (2018).
- T. Zapletal, P. Sperka, I. Krupka, M. Hartl, The effect of surface grooves on transition to mixed lubrication. *Tribol. Int.* **114**, 409–417 (2017).
- J. Bonaventure, J. Cayer-Barrio, D. Mazuyer, Transition between mixed lubrication and elastohydrodynamic lubrication with randomly rough surfaces. *Tribol. Lett.* **64**, 44 (2016).
- J. Guegan, A. Kadiric, A. Gabelli, H. Spikes, The relationship between friction and film thickness in EHD point contacts in the presence of longitudinal roughness. *Tribol. Lett.* **64**, 33 (2016).
- S. Bair, Y. Liu, Q. J. Wang, The pressure-viscosity coefficient for Newtonian EHL film thickness with general piezoviscous response. *J. Tribol.* **128**, 624–631 (2006).
- H. van Leeuwen, The determination of the pressure viscosity coefficient of a lubricant through an accurate film thickness formula and accurate film thickness measurements. *J. Eng. Tribol.* **223**, 1143–1163 (2009).
- A. L. Demirel, S. Granick, Glasslike transition of a confined simple fluid. *Phys. Rev. Lett.* **77**, 2261–2264 (1996).
- E. Bayart, I. Svetlizky, J. Fineberg, Slippery but tough: The rapid fracture of lubricated frictional interfaces. *Phys. Rev. Lett.* **116**, 194301 (2016).
- C. Allain, J. Piard, A. Brosseau, M. Han, J. Paquier, T. Marchandier, M. Lequeux, C. Boissière, P. Audebert, Fluorescent and electroactive low-viscosity tetrazine-based organic liquids. *ACS Appl. Mater. Interfaces* **8**, 19843–19846 (2016).
- D. Petrova, B. Weber, C. Allain, P. Audebert, D. Bonn, A. M. Brouwer, Fast 3D microscopy imaging of contacts between surfaces using a fluorescent liquid. *ACS Appl. Mater. Interfaces* **10**, 40973–40977 (2018).
- B. Weber, T. Suhina, T. Junge, L. Pastewka, A. M. Brouwer, D. Bonn, Molecular probes reveal deviations from Amontons' law in multi-asperity frictional contacts. *Nat. Commun.* **9**, 888 (2018).
- J. A. Greenwood, J. H. Tripp, The contact of two nominally flat rough surfaces. *Proc. Inst. Mech. Eng.* **185**, 625–633 (1970).
- B. N. J. Persson, *Sliding Friction* (Springer, ed. 2, 2000).
- I. A. Lyashenko, A. E. Filippov, M. Popov, V. L. Popov, Effect of stress nonhomogeneity on the shear melting of a thin boundary lubrication layer. *Phys. Rev. E* **94**, 053002 (2016).
- J. B. Clark, J. W. Hastie, L. H. E. Kihlberg, R. Metselaar, M. M. Thackeray, Definitions of terms relating to phase transitions of the solid state (IUPAC Recommendations 1994). *Pure Appl. Chem.* **66**, 577–594 (1994).
- K. Simonovic, M. Kalin, Experimentally derived friction model to evaluate the anti-wear and friction-modifier additives in steel and DLC contacts. *Tribol. Int.* **111**, 116–137 (2017).
- D. S. Kammer, I. Svetlizky, G. Cohen, J. Fineberg, The equation of motion for supershear frictional rupture fronts. *Sci. Adv.* **4**, eaat5622 (2018).
- P. E. Milner, M. Parkes, J. L. Puetzer, R. Chapman, M. M. Stevens, P. Cann, J. R. T. Jeffers, A low friction, biphasic and boundary lubricating hydrogel for cartilage replacement. *Acta Biomater.* **65**, 102–111 (2018).
- J. Faivre, B. R. Shrestha, G. Xie, M. Olszewski, V. Adibnia, F. Moldovan, A. Montembault, G. Sudre, T. Delair, L. David, K. Matyjaszewski, X. Banquy, Intermolecular interactions between bottlebrush polymers boost the protection of surfaces against frictional wear. *Chem. Mater.* **30**, 4140–4149 (2018).
- A. Zuin, T. Cousseau, A. Sinatora, S. H. Toma, K. Araki, H. E. Toma, Lipophilic magnetite nanoparticles coated with stearic acid: A potential agent for friction and wear reduction. *Tribol. Int.* **112**, 10–19 (2017).
- D. F. Kienle, T. L. Kuhl, Analyzing refractive index profiles of confined fluids by interferometry. *Anal. Chem.* **86**, 11860–11867 (2014).
- B. A. Weber, thesis, University of Amsterdam (2017).
- J. H. Snoeijer, J. Eggers, C. H. Venner, Similarity theory of lubricated Hertzian contacts. *Phys. Fluids* **25**, 101705 (2013).
- S. Hyun, L. Pei, J. F. Molinari, M. O. Robbins, Finite-element analysis of contact between elastic self-affine surfaces. *Phys. Rev. E Stat. Nonlin. Soft Matter Phys.* **70**, 026117 (2004).
- N. Otsu, A threshold selection method from gray-level histograms. *IEEE Trans. Syst. Man Cybern.* **9**, 62–66 (1979).
- B. Weber, T. Suhina, A. M. Brouwer, D. Bonn, Frictional weakening of slip interfaces. *Sci. Adv.* **5**, eaaw7603 (2019).

Acknowledgments

Funding: This research was financially supported by the Netherlands Organization for the Advancement of Research (NWO). **Author contributions:** D.P. performed experimental work and analysis. C.H.V. contributed to theoretical work. D.B. and B.W. contributed to the analysis. C.A. and P.A. synthesized the fluorescent liquid. All authors contributed to the writing of the manuscript. **Competing interests:** The authors declare that they have no competing interests. **Data and materials availability:** All data needed to evaluate the conclusions in the paper are present in the paper and/or the Supplementary Materials. Additional data related to this paper may be requested from the authors.

Submitted 23 December 2018

Accepted 21 October 2019

Published 6 December 2019

10.1126/sciadv.aaw4761

Citation: D. Petrova, B. Weber, C. Allain, P. Audebert, C. H. Venner, A. M. Brouwer, D. Bonn, Fluorescence microscopy visualization of the roughness-induced transition between lubrication regimes. *Sci. Adv.* **5**, eaaw4761 (2019).

Fluorescence microscopy visualization of the roughness-induced transition between lubrication regimes

Dina PetrovaBart WeberClem ence AllainPierre AudebertCees H. VennerAlbert M. BrouwerDaniel Bonn

Sci. Adv., 5 (12), eaaw4761.

View the article online

<https://www.science.org/doi/10.1126/sciadv.aaw4761>

Permissions

<https://www.science.org/help/reprints-and-permissions>

Use of think article is subject to the [Terms of service](#)

Science Advances (ISSN 2375-2548) is published by the American Association for the Advancement of Science, 1200 New York Avenue NW, Washington, DC 20005. The title *Science Advances* is a registered trademark of AAAS.

Copyright   2019 The Authors, some rights reserved; exclusive licensee American Association for the Advancement of Science. No claim to original U.S. Government Works. Distributed under a Creative Commons Attribution NonCommercial License 4.0 (CC BY-NC).